The Effects of Waste Materials on the Thermo-mechanical Properties of Eco-Friendly Bricks

Şermin Koçyiğit[1]

Abstract

The world is now obliged to produce sustainable, green and environmentally friendly construction materials to improve thermal comfort in buildings, reduce energy costs, and alleviate the effects of both greenhouse gas emissions and global warming. In this study, the researcher produced cost-effective eco-friendly construction materials with higher effective thermal conductivity using two alkaline activators (AA), sodium hydroxide (NaOH) and sodium silicate (Na_2SiO_3), in combination with waste materials including a regional volcanic rock Diyarbakır Karacadağ Red Scoria (KS) and Karacadağ rice husk ash (RHA). First, the researcher analysed the raw materials through Particle Size analysis, XRF, XRD, TGA/DTA, SEM, and EDS to determine their characteristics. Then, they were mixed at different rates to form mixtures (clay: 65 %, 60 %, 55 %, 55 %, and 50 %; KS: 30 % (fixed); RHA: 5 %, 10 %, 15 %, and 20 %; AA: 5 %, 10 %, and 15 %). Rectangular samples for mechanical tests and cylindrical samples for thermal tests were made and fired at 950 °C. Next, SEM, EDS and XRD analyses were carried out on the fractured bricks after they were tested for compressive strength. Then, the researcher analysed the fired bricks for their bulk density, apparent porosity, water absorption, compressive strength, loss on ignition, effective thermal conductivity, and microstructures. Experimental results demonstrated that porosity, water absorption, and loss on ignition increased. However, density, compressive strength, and effective thermal conductivity decreased as the rates of RHA and NaOH + Na_2SiO_3 increased with Karacadağ scoria at a fixed rate. The addition of waste RHA, KS, and AA in the brick yielded in a significant improvement in thermal performance (by 0.263 W·mK^{-1}) compared to the control bricks (1.043 W·mK^{-1}), while the compressive strength dropped from 32.5 MPa to 7.2 MPa. Even though the compressive strength decreased due to the micropores forming as a result of the addition of these materials in the brick, it was greater than 7MP, as stated in the literature. The findings of this study indicated that the fired clay bricks produced are potential materials for construction applications that require an appropriate thermal insulation and mechanical strength, as well as internal structural applications.

Extended author information available on the last page of the article

1 Introduction

In recent years, rapid urbanisation due to growing populations has led a huge demand for building construction, and thus for concrete and bricks. Both materials shelter people and provide thermal comfort in interior spaces. Air conditioners, fans, and other mechanical and electrical cooling devices used for air conditioning of uninsulated buildings lead to energy consumption, greenhouse gas, and carbon emissions. Buildings account for about 40 % of the total energy consumed in the world and 33 % of total global carbon dioxide emissions [1]. Heating and cooling are responsible for more than 50 % of the total energy consumed in buildings. Many people have attempted to reduce energy consumption and their carbon footprint by opting for appropriate materials, alternative designs, and exterior cladding that provide adequate thermal insulation [2–4]. Approximately 30 % of the energy and heat losses in buildings are caused by walls and roofs; therefore, it is needed to reduce heat loss and maintain thermal comfort [5]. Clay bricks are widely used in construction around the world—with fired clay bricks being the oldest known and most preferred building material [6, 7]. Fired clay bricks offer the construction sector many advantages: they are affordable for production and maintenance, they have suitable mechanical properties, and they are durable, excellent thermal insulators, and easy to build with [8]. One can also add pore-forming or low thermal conductivity materials to the raw clay to improve their thermal insulation properties, hence cutting down on ultimate energy consumption and costs [9].

Diyarbakır Karacadağ red scoria (aka Karacadağ slag (KS)) is a basic pumice scoria. Made from lava, it is resistant to physical and chemical wear, contains numerous pores, and has very high thermal and sound insulation. In contrast to pumice, KS is basic due to its low content of silicon oxide. It is commonly used to make cement and pozzolan, for road construction, and as an adsorbent. Its effective use depends on its physical and chemical properties. Therefore, the characterisation of KS is not only a matter of scientific analysis, but also of critical importance in the practice [10, 11]. In recent years, the notions of "recycle, recover, reduce, and reuse" are critical for having a sustainable future. Therefore, the use of KS as a waste material in construction applications is important for the environment.

Agricultural products generates lots of natural waste, during both harvesting and after consumption, namely: leaves, stalks, straw, and ash. Most of them get disposed of into environment or incinerated [12]. They also are a source of environmental pollution. Hence, clay-based bricks are used in large quantities worldwide; moreover, converting industrial and agricultural waste into fired clay bricks seems to be an ideal way to improve sustainability. The more agricultural or industrial waste and less clay you use to make the brick, the lighter clay brick, thereby increasing energy efficiency [13]. Numerous kinds of agricultural as well as industrial waste have been used to improve the mechanical and thermal insulation properties of fired clay bricks. Among these include: rice husk bran [14, 15], wheat straw [16, 17],

tea waste [6, 18], date palms [19], olive kernel flour [16], rice husk ash (RHA) [20, 21], waste glass sludge [22], chemical coke [23], rubber waste [24], and ferrochrome slag [25]. The United States, China, Africa, and India all use rice husks as biomass to generate electricity [26].

The use of RHA in construction materials offers several advantages due to its pozzolanic nature. They reduce the permeability of these materials, they make them more resistance to chemical impacts and alkali-silica reaction, and improve their workability, and they increase the strength of the construction material [27–32]. It also can reduce the unit weight of the clay brick, improve its thermal properties, and increase pore volume in the clay structure. Therefore, clay bricks featuring RHA are good for the economy and energy efficiency.

Sodium hydroxide (NaOH) is widely used as an alkali activator (AA) in geopolymers. The properties of the resulting mortar are determined by the density and molarity of the activating solution. The addition of high quantities of NaOH accelerates chemical dissolution and adversely affects the structure of ettringite and CH during binder formation. Sodium silicate (Na_2SiO_3), on the other hand, is commonly incorporated into construction materials as a set accelerator.

This study covers the recycling of natural waste materials such as KS waste powder and rice husk by using them in building materials in terms of environmental sustainability and evaluation of factory areas. In the literature, there are studies on the production of plaster mortars, geopolymer concrete and lightweight concrete using various wastes, cement and NaOH or Na_2SiO_3 separately as sintering aid. However, there have been no studies on the synergistic effect of the regional Diyarbakır Karacadağ Scoria together with the local RHA and the use of both chemicals ($NaOH + Na_2SiO_3$) as sintering aids on the properties of the fired brick. The originality of this study is to produce low-cost, heat-insulating, environmentally friendly, lightly fired clay bricks instead of lightweight concrete or plaster mortar, which has a high carbon dioxide content and is high cost.

2 Materials and Methods

The methodology includes for what purpose the samples produced by mixing the raw materials at different rates according to the physical, chemical, and mineralogical analyses can be used in the buildings according to the results of the mechanical, physical and effective thermal conductivity tests. KS waste powder acted as both aggregate and pore former in the sample. The raw clay served as a binder. It was thought that RHA would produce pores due to its amorphous structure and specific surface size, while NaOH and sodium silicate would be sintering additives. Figure 1 shows the raw materials used in the study.

Before production, the researcher subjected the raw materials to pre-treatments such as crushing, drying, grinding, and ashing (RHA) and then analysed their particle size, chemical, thermal, mineralogical, and microstructural analyses.

The chemical compositions of the raw materials were investigated using X-Ray Fluorescence (XRF) spectroscopy on a Spectro Xepos II (50 kV and 0.7 mA). Next, the researcher examined their thermogravimetric and differential thermal

Fig. 1 Clay, Karacadağ red scoria (KS), and RHA raw materials, sodium silicate (Na_2SiO_3) and NaOH alkali activators

properties (TG/DTA) under nitrogen atmosphere (50 ml·min^{-1}) using a Hitachi STA 7300 thermal analyser, which can operate between room temperature up at 1000 °C at a heating rate of 10 °C·min^{-1}.

The X-ray diffraction patterns of the raw materials and clay bricks were recorded on a Rigaku miniflex600 diffractometer. The researcher irradiated the samples from Cu-Kα radiation at 40 kV and 15 mA. Additionally, XRD analyses were done at a wavelength of 1.5406 (λ) between 10° and 90° at a scanning speed at 2° per minute.

The microstructural morphology of the raw material and clay bricks was analysed on a Hitachi SU3500 digital SEM (scanning electron microscope of various scales) with an accelerating voltage of 20 kV. The researcher then carried out energy dispersive X-ray spectroscopy (EDS, Oxford INCA X-ray spectrometer) on the regions of the clay bricks that were scanned in the SEM analysis.

Using a pycnometer, the researcher detected that the densities of brick raw material, KS waste powder, and rice husk were 1.16 g·cm^{-3}, 1.07 g·cm^{-3}, and 1.02 g·cm^{-3}, respectively.

The rice husk was turned into ash in an industrial furnace at 800 °C for 2 h, and then ground down into a particle size of less than 75 μm. The clay and KS waste powder were ground into a particle size of less than 150 μm. Later, the researcher prepared 5–10–15 % solutions by dissolving 50, 100, and 150gr granular NaOH in 1000 ml distilled water, respectively. She also prepared a solution of 5–10–15 % by mixing 50, 100, 150 ml Na_2SiO_3 with 1000 ml distilled water. She prepared a control mixture (A0) that did not feature RHA, KS, or AA. Table 1 shows the mixture ratios of the samples. The samples were mixed in a mechanical stirrer for 5 min until a homogeneous mixture was obtained. Each homogenised composition was poured into 40 mm × 40 mm × 160 mm rectangular steel moulds for mechanical tests and in 50 mm × 30 mm cylindrical plastic moulds for thermal tests, and then pressed uniaxially at 10 N·mm^{-2}.

The pressed samples were left to sit in the moulds at room temperature for a day. The researcher then removed them from the moulds and placed them in a Protherm PLF12/25 oven to dry at 40 °C for 24 h, and then at 105 °C for another 4 h. Shen then fired them at 950 °C for 2 h at a heating rate of 10 °C·min^{-1}. Figure 2 shows the fired clay bricks in groups.

Table 1 Mixture rates of the samples

Group	Code	Clay (%)	RHA (%)	KS (%)	NaOH + Na$_2$SiO$_3$ (%)	Uncertainty (%)
G1	A0	100%	0	0	0	Control sample
	A1	65	5	30	5	11
	A2	60	10	30	5	10.12
	A3	55	15	30	5	8.42
	A4	50	20	30	5	7.31
G2	B1	65	5	30	10	10.55
	B2	60	10	30	10	9.15
	B3	55	15	30	10	7.83
	B4	50	20	30	10	6.61
G3	C1	65	5	30	15	10.17
	C2	60	10	30	15	8.71
	C3	55	15	30	15	7.31
	C4	50	20	30	15	5.99
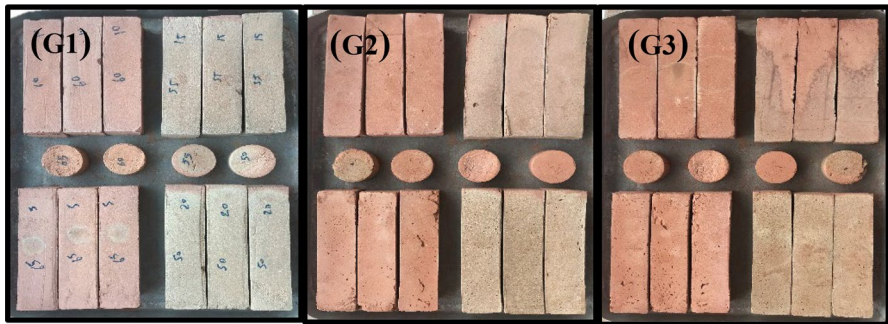
Fig. 2 Grouped fired clay brick samples (G1, G2, G3)

Manual callipers were used to measure changes in the linear shrinkage (LS) of the samples after the drying and firing steps. The total linear shrinkage of the samples was determined according to TS 4790 [33].

Brick characteristics of the produced brick samples were observed. Loss on ignitions (LOI) of the bricks was evaluated by the weight changes thereof before and after the firing process [8]. Physical properties such as bulk density, apparent porosity, and water absorption were determined in accordance with the ASTM C20 standard. Compressive strength tests were carried out at a 0.5 mm·min^{-1} load on a BZ 701/120 mechanical testing machine with a capacity of 100 kN based on TS EN 772–1 standard. The device can measure the compressive strength within an accuracy of 1 %. The researcher also measured effective thermal conductivity of the samples were on a C-Therm TCi device (developed according to ASTM D7984-16). According to the device catalogue, the device measures thermal conductivity with

an uncertainty of 5 % and the measurement range of 0.02–200 Wm^{-1} K^{-1}. The operating principle of the device (TCi) is based on conductors in series with respect to the direction of heat flow. This method is used to measure the effective thermal conductivity coefficient without affecting the humidity in the samples. What makes this method different from the plate type effective thermal conductivity coefficient measurement method is that one can still make measurements even when the medium of the effective thermal conductivity coefficient is heterogeneous [9]. The researcher measured each sample at least three times at different locations and used the arithmetic mean of the results in the study. Figure 3 shows methodology used by the researcher to produce and test the fired bricks.

3 Results and Discussion

3.1 Characterisation of the Raw Materials

3.1.1 Chemical Composition of the Raw Materials

Table 2 shows the results of XRF applied to determine the chemical and oxide composition of the raw materials. RHA was categorised as a Type F pozzolan in
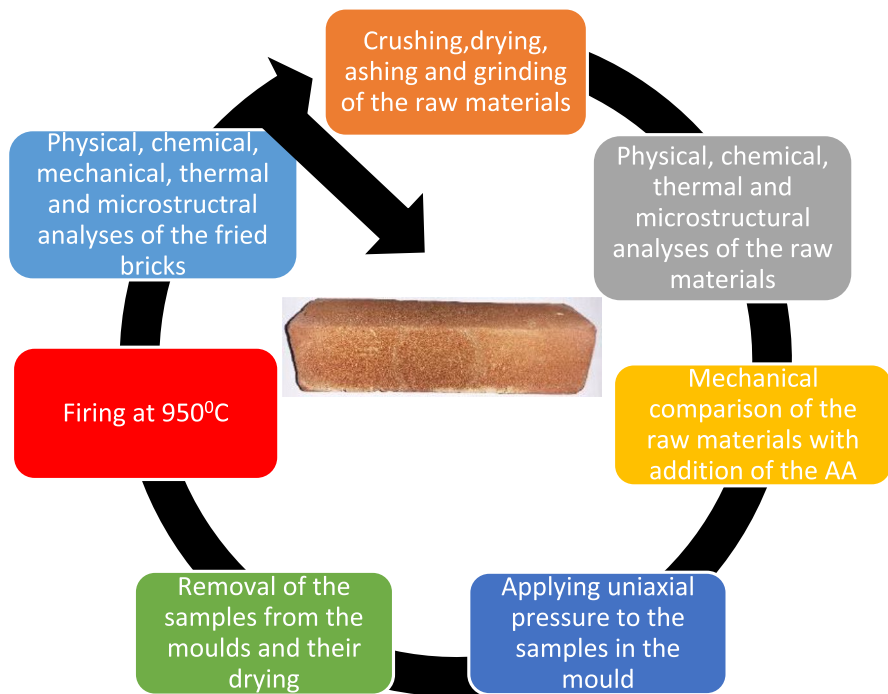

Fig. 3 Methodology of production and testing

Table 2 Chemical composition of the raw materials (wt%)

Compounds	Clay (%)	Karacadağ Scoria (%)	Rice husk ash (%)
SiO_2	51.50	41.83	79.165
Al_2O_3	17.12	14.873	1.612
Fe_2O_3	9.91	16.760	1.862
MgO	6.86	5.768	2.253
CaO	9.46	9.80	6.404
Na_2O	1.01	3.878	0.220
K_2O	2.28	1.966	9.292
TiO_2	0.997	3.203	0.205
MnO	0.165	0.230	0.161
SO_3	0.051	0.451	2.261
P_2O_5	0.182	0.779	2.985
LOI	5.35	8.28	4.12
Uncertainty (%)	5.26	5.51	2.69

accordance with the ASTM C618 standard. LOI of 4.12 indicates that the amount of unburned carbon was low, hence high pozzolanic activity could be achieved.

3.1.2 Particle Size Analyses of the Raw Materials

Figure 4 shows the particle size distribution of the raw materials. The average particle sizes of clay, KS waste powder, and waste rice husk ash were approximately 72.8, 87.31, and 77.55 μm, respectively. Clay and KS waste powder contained particles as small as 150 μm, while rice husk ash contained particles smaller than 100 μm. The rates of fine clay and fine KS waste powder particles in the clay/KS waste powder was higher than the rate of the waste RHA. The clay and KS waste powder used in this study both contain a high amount of microparticles that bond well RHA particles. The rate of clay particles passing through the 150 μm sieve was 53.74 %; the rate of KS waste powder particles was 51.18 %; and the rate of RHA particles passing through the 75 μm sieve was 48.87 %. This indicates that clay, KS waste powder, and RHA samples were composed of fine particles. Fine KS waste powder and RHA particles moved very easily between clay particles. Consequently, the KS waste powder and RHA were mixed very well with the clay.

3.1.3 XRD Analyses of the Raw Materials

Figure 5a–c show the X-ray diffraction (XRD) analysis of clay, KS waste powder, and rice husk ash, respectively. Accordingly, the clay raw material mainly contained the quartz (SiO_2), muscovite, albite, zussmanite, and calcite ($CaCO_3$) phases. KS waste powder predominantly contained hematite, muscovite, anorthite, cristobalite, diopside, and amorphous material—in that order of quantity (high to low). Combustion removed organic part of the rice husk, and left behind a residue rich in silica.
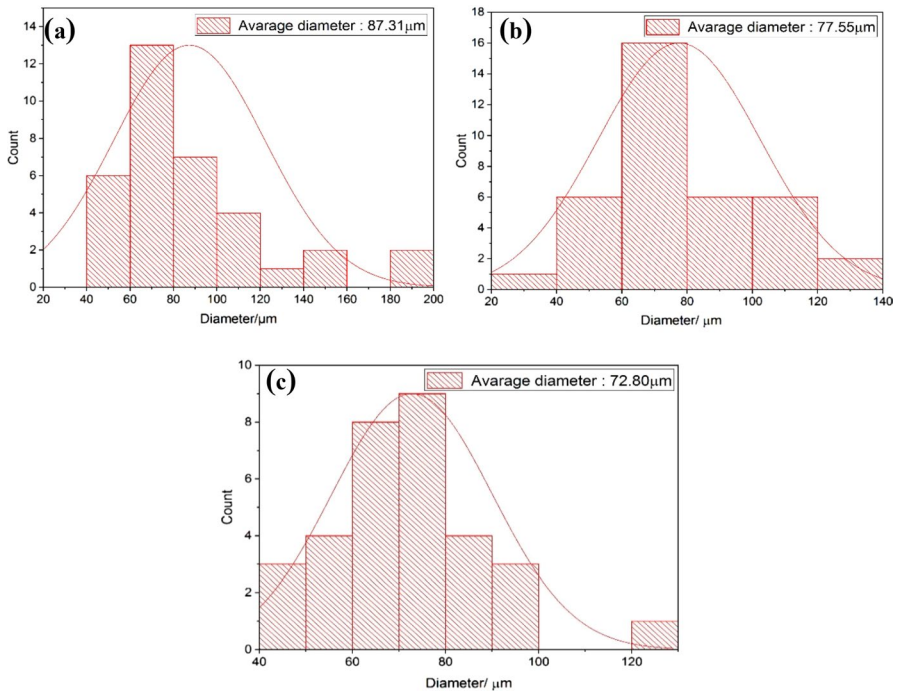
Fig. 4 Particles sizes of the raw materials: (a) Clay, (b) KS and (c) RHA

The soluble fraction of silica for the waste RHA sample from the oven was 83.2 %; demonstrating that SiO_2 in waste RHA was more amorphous and reactive.

3.1.4 TGA/DTA Analyses of the Raw Materials

Figure 6 shows the TGA curves of clay, KS waste powder and RHA. Accordingly, the researcher observed a total weight loss approximately 15 % (red curve) after it was heated to 1100 °C. Three basic reactions occurred: (1) the evaporation of physical water up to 100 °C, (2) dehydration of hydroxyl-containing clay compounds between 350 °C and 500 °C, and (3) decomposition of the small amount of calcium carbonate after 600 °C and after the removal of CO_2 from the structure. Likewise, in KS, the total weight loss is about 11 %. The sample lost only 2 wt% up to 100 °C, which was attributed to the absorbed water in the slag. According to the XRD analysis, the muscovite phase in the sample content began to decompose at 760 °C and the hydroxyl structure in its structure decomposed. A weight decrease was detected upon the removal of the chemically bound hydroxyl from the structure. The decomposition reaction (weight decrease) in the TGA curve after 760 °C was nearly reached the thermal properties of an ideal muscovite mineral. A wide temperature range for dehydroxylation (760 °C–1000 °C) may be associated with the wide distribution of the thermal response of hydroxyls. Moreover, in RHA, a total weight loss of approximately 25.1 % was observed when heated to 1150 °C. Referring to
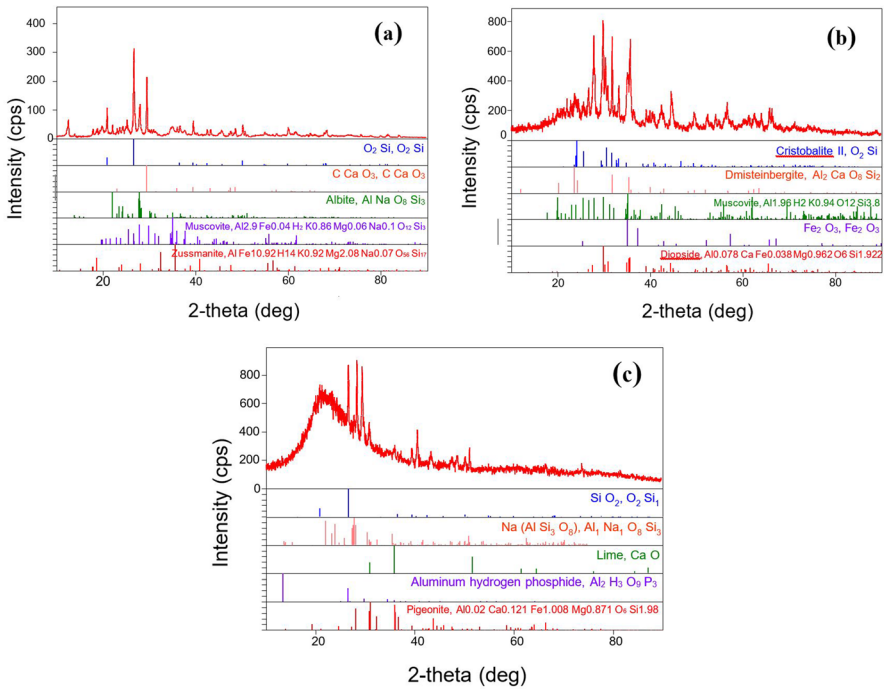
Fig. 5 XRD images of the raw materials: (a) Clay, (b) KS, and (c) RHA

the DTA curve, mainly two major exothermic reactions took place between 500 °C and 1000 °C, corresponding to the burning of the rice husk.

3.1.5 SEM Analyses of the Raw Materials

Figure 7a–c show SEM images of the particle morphologies of the raw materials. Figure 7a shows that the clay raw material had a micron-size stratified particle structure, and it had agglomerated. Sub-micron and micron-size particles were also observed in the morphology of agglomerated powders, as were micron porous structures at varying diameters (Fig. 7b and c). Waste RHA was nested and agglomerated.

3.2 Characterisation of the Brick Samples After Firing

3.2.1 Linear Shrinkage and Loss of Bulk Density

To find out how the conventional sintering process affected the samples, one must first perform the characterisation of their physical properties through loss of linear shrinkage (LS) and bulk density (BD) [20]. To determine the loss of LS, the researcher carried out several unidimensional measurements on the diameter of the cylindrical samples with the manual calliper. She then calculated the loss of LS by
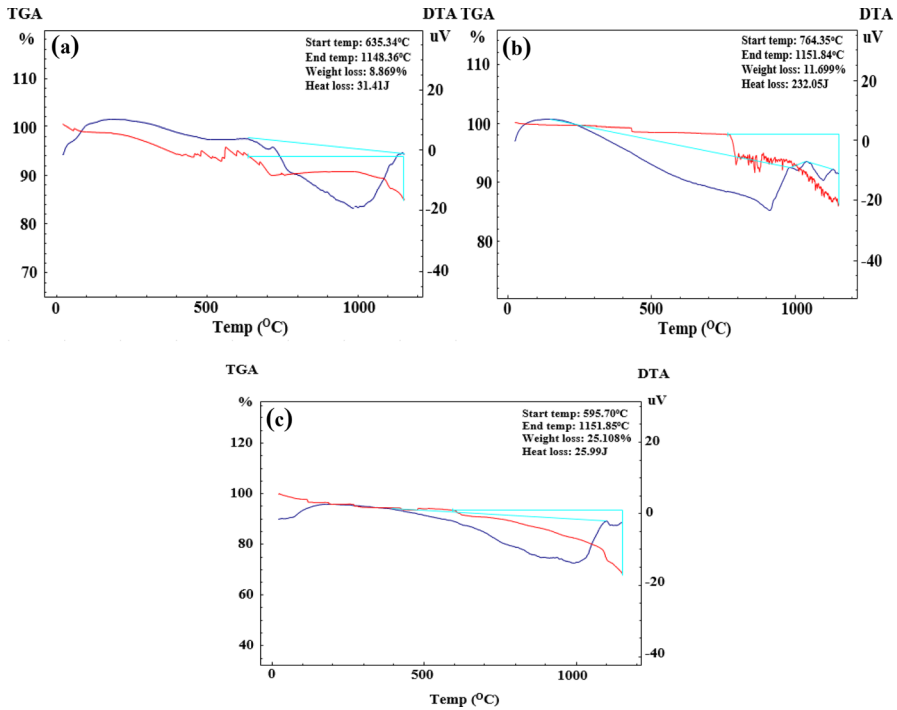
Fig. 6 TGA/DTA images of the raw materials: (a) clay, (b) KS, and (c) RHA

determining the pre-sintering diameter of the compacted sample (L_0) and the post-sintering diameter of the compacted sample (L_1) and using Eq. 1 below. She then calculated their densities based on their pre-sintering mass (m) and volume (V), and using Eq. 2. The post-sintering densities were then determined according to ASTM C20.

The loss of BD was calculated by measuring the pre- sintering density (p_0) and the post-sintering density of the sample (p_1), and then entering that into Eq. 3.

$$\text{LS} = \frac{L_0 - L_1}{L_0} \times 100\,\% \tag{1}$$

$$\rho = m/V \tag{2}$$

$$\rho_1 = \frac{\rho_0 - \rho_1}{\rho_0} \times 100\,\% \tag{3}$$

Figure 8 shows the LS and BD loss of the bricks. Samples that had more RHA and KS also had a higher LS and loss of BD. The linear shrinkage varied between 2.3 % and 4.7 %, whereas the loss of bulk density varied between 21 % and 38 %. This was caused by the SiO_2 crystals in the RHA and KS, and possibly the cristobalite crystal—which, in turn, leads to higher shrinkage and loss of densification
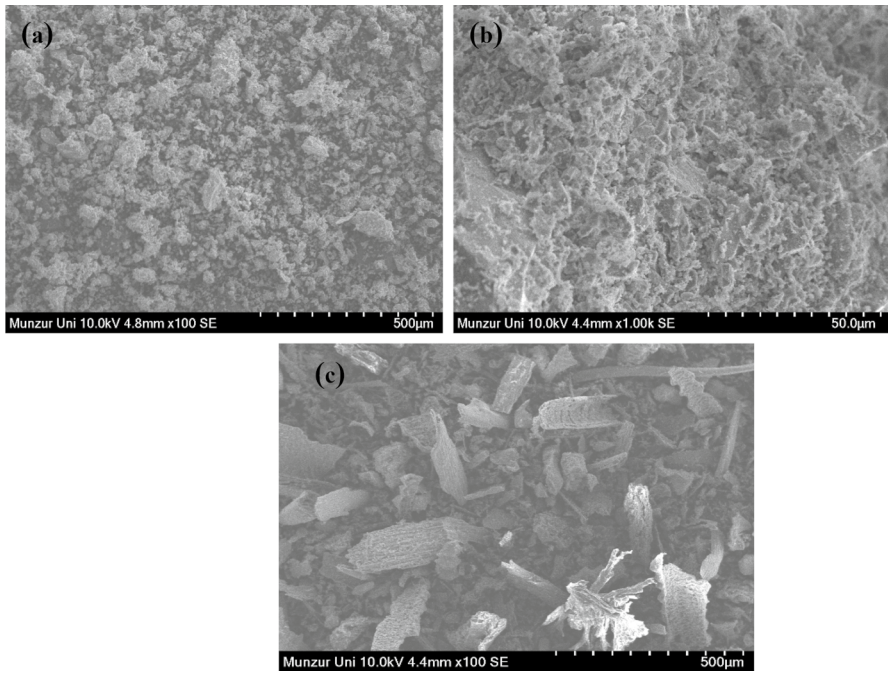
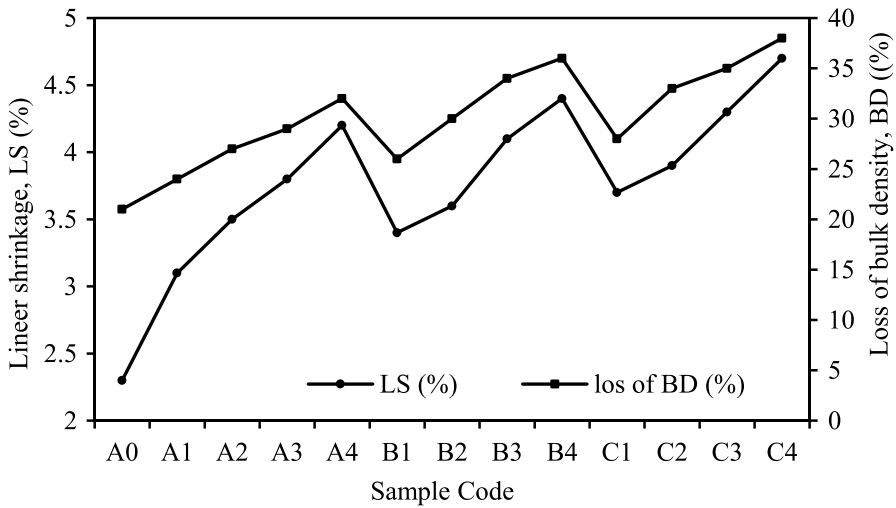**Fig. 7** SEM images of the raw materials: (a) clay, (b) KS, (c) RHA

Fig. 8 LS and loss of BD of the samples because sintering at 950 °C for 2 h

due to the higher RHA and KS content. Moreover, higher RHA and KS content resulted in more gaps, thereby causing the radius of the sintered samples to shrink more linearly. Additionally, the more sintering additives the samples contained, the

better they sintered (Fig. 2). The researcher also obtained light clay bricks by adding a fixed rate of KS waste powder and various rates of RHA. Therefore, C4 was the lightest sample while A1 was the heaviest sample.

3.2.2 Bulk Density

The thermal, mechanical, and physical properties of the samples were all affected by the density of the materials. Volume, density, mixing rates, firing temperatures of its components likewise determine the density of the brick. Denser bricks limit the absorbing capacity, thus reducing water absorption, and enhancing mechanical performance.

The researcher used Eq. 4 to find out the bulk densities (ρ_b) of the fired clay bricks. First, she calculated the dried weight (W_1) of the samples, then the soaked weight (W_2) (by soaking them in water for 3 h), and finally the weight suspended in water (W_3) using a spring suspension balance. In Eq. 4, ρ_w is the density of water ($g \cdot cm^{-3}$).

$$\rho_b = W_1 \times \rho_w / W_2 - W_3 \tag{4}$$

The bulk densities of fired clay bricks are listed in Table 3 and shown in Fig. 9a. Figure 9b, c show the correlations between bulk density, apparent porosity and waste contents. As seen in the figure, a negative correlation was observed between bulk density, apparent porosity and waste content. The comparison of the bulk density of the bricks containing KS waste powder and RHA with the control brick (A0) is shown in percent on the bars in the figure. Bulk density values vary between 1.29 $g \cdot cm^{-3}$ and 1.91 $g \cdot cm^{-3}$. The researcher observed a significant drop in the densities as the rates of RHA and AA increased with KS waste powder at a fixed rate (by weight). The fired clay bricks had adequate densities (less than 2.0 $g \cdot cm^{-3}$) in accordance with the relevant standards (ASTM C469, ACI 213 and BS EN 206-1), that are recommended for structural applications. It is beneficial to reduce the bulk density in structural applications. Another point about the results is that the sample bricks had a competitive lightness compared to the unit weight values of other bricks in the literature (Table 4).

3.2.3 Apparent Porosity

The apparent pores of fired clay bricks are listed in Table 3 and shown in Fig. 10a. The apparent pores (P) of the samples were determined using Eq. 5.

$$P = W_2 - W_1 / W_2 - W_3 \tag{5}$$

The porosity changes of the bricks containing waste RHA and KS—compared to the control brick (A0)—were presented as percentages on the bars in Fig. 10. The values varied between 30.6 % and 47.8 %. The pores of the bricks showed a significant increase with the addition of RH, KS, and AA. Compared to control brick (A0), a maximum increase (approximately 56.21 %) in apparent porosity of the samples was obtained at 20 wt%, 30 wt% KS and 15 wt% AA (C4). A minimum

Table 3 The test results of the bricks

| Group	Code	Clay (%)	RHA (%)	KS (%)	NaOH+Na$_2$O$_3$ (%)	Bulk Density (g·cm^{-3})	Porosity (%)	TC (W·mK^{-1})	WA (%)	CS (Mpa)	Loss on ignition (wt%)
G1	A0	100	0	0	0	1.91	30.6	1.043	12.1	32.5	5.1
	A1	65	5	30	5+5	1.82	35.9	0.735	16.7	18.3	6.3
	A2	60	10	30	5+5	1.71	38.7	0.687	20.3	13.7	7.6
	A3	55	15	30	5+5	1.65	41.3	0.558	24.5	11.2	8.4
	A4	50	20	30	5+5	1.53	43.6	0.443	26.4	9.2	9.1
Uncertainty						0.07	3.23	0.1	3.91	4.37	0.72
G2	B1	65	5	30	10+10	1.75	37.5	0.602	19.7	17.4	7.4
	B2	60	10	30	10+10	1.62	39.8	0.514	22.2	12.8	8.2
	B3	55	15	30	10+10	1.51	43.4	0.421	25.8	9.7	9.3
	B4	50	20	30	10+10	1.45	45.2	0.356	28.3	8.1	10.2
Uncertainty						0.08	3.75	0.12	5.15	4.57	0.88
G3	C1	65	5	30	15+15	1.67	38.7	0.523	21.8	13.3	8.3
	C2	60	10	30	15+15	1.49	41.6	0.401	24.2	10.6	9.7
	C3	55	15	30	15+15	1.41	45.9	0.322	26.9	8.3	10.5
	C4	50	20	30	15+15	1.29	47.8	0.263	28.4	7.2	11.7
Uncertainty						0.11	5.07	0.14	6.99	4.98	1.13
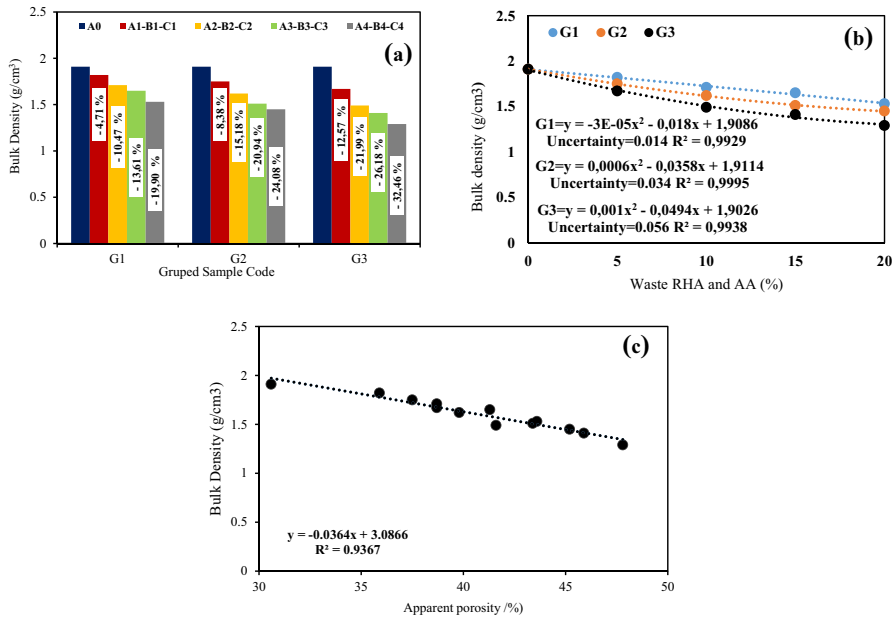
Fig. 9 Density of the samples according to mixing rates and correlation

increase (approximately 17.32 %) was obtained at 5 wt% RHA, 30 wt% KS, and 5 wt% AA (A1). Porosity significantly affects the physical, mechanical, and thermal characteristics of construction materials, including compressive strength, unit weight, and thermal conductivity. The more the researcher added RHA, KS, and AA content, the more pores they obtained in the samples. Here are few possible reasons for this: the porosity of RHA, the size of its specific surface, its amorphous structure, and the increase in unreacted material in the brick. Figure 10b shows the correlations between experiments and waste contents. A positive linear correlation was observed between apparent porosity and waste content. The range of apparent porosity the researcher obtained in this study was close to the average when compared to other values obtained from the literature (Table 4). Porosity had an important effect on numerous properties of the bricks. Figures 10, 11, 1300 and 1400 all show an increase in the apparent porosity that ultimately raised the water absorption capacity and decreased bulk density, compressive strength, and effective thermal conductivity.

3.2.4 Water Absorption

Water absorption values of the samples are listed in Table 3 and shown in Fig. 11a. Figure 11b, c show the correlations between water absorption, apparent porosity and waste contents. As seen in the figure, water absorption had a positive linear correlation with apparent porosity and waste content. Water absorption tests were conducted on the porous samples by boiling them in water at 100 °C for 2 h, and then soaking them in water for additional 4 h. Water absorption

Table 4 A summary of the literature on clay bricks and their findings in contrast to this study

Materials content	Usage ratio (%)	Bulk density (g·cm^{-3})	Apparent porosity (%)	Effectiv thermal conductivity (W·mK^{-1})	Water absorption (%)	Compressive strength (MPa)	References
SWW	5–17.5	1.68–1.86	56–74	0.42–0.54	16–20	13–27	[34]
SWTP/RSA/SBA/WSA	5–15	1.44–1.63	22–29	–	35–40	12–15	[35]
SS/FA/OS	5–10	1.62–1.75	21–27	0.7 (approx.)	11–13	–	[36]
SDW	2.5–10	1.41–1.83	22–32	0.47–0.22	12–22	4–18	[37]
TW/SD/WS	2–4/2–6/1–2	1.36–1.68	29–37	0.38–0.48	17–24	6–13	[38]
BA	5–20	1.59–1.62	31–35	–	20 (approx.)	7–46	[39]
HCWPAN/WCC/YCC	10–40	1.61–2.32	15–33	0.155–0.34	8.9–18.2	2–4	[40]
SW/SS/WA/BA	5–20	1.43–1.73	15–27	–	12–17	3–11	[41]
WMS	5–25	–	17–42	0.47–0.56	15–23	4–9	[42]
MCW	5–25	1.92–1.97	23–32	0.77–1.00	11–13	7–28	[43]
OPBA	5–20	1.43–1.52	18–34	0.33–0.41	16–28	9–11	[44]
VS	5–11–17	1.12–1.68	28–41	0.28–0.738	16–36	1.5–38	[45]
CC/WG	10/5–20	1.44–2.18	16–34	0.57–0.81	10–20	5–19	[46]
GT/PD	2.5–15	1.42–1.91	38–41	0.29–0.37	14–33	3–21	[47]
KS/RHA	30/5–20	1.29–1.91	30.6–47.8	0.263–0.735	12.1–28.4	7.2–32.5	This study

Explanation of abbreviations

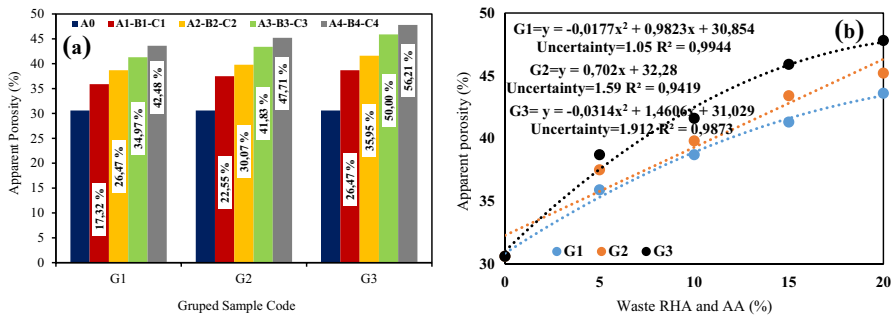|	
SWW: Stone Wool Waste	MCW: Marble Cutting Waste
SWTP: Sludge of Water Treatment Plants	OPBA: Olive Pomace Bottom Ash
RSA: Rice Straw Ash	VS: Vine Shoots
SBA: Sugar Cane Bagasse Ash	CC: Corn Cob
WSA: Wheat Straw Ash	WG: Waste Glass
SS: Sewage Sludge	GT: Grapevine Twig
FA: Fly Ash	PD: Poplar Dust
OS: Oven Slag	WCC: White Clay Matrix
SDW: Sawdust Waste	YCC: Yellow Clay Matrix
TW: Tea Waste	SW: Sawdust Waste
SD: Tea Waste	SS: Steel Sludge
WS: Wheat Straw	WA: Wood Ash
BA: Bone Ash	BA: Banana Ash
HCWPAN: Hydrothermally Calcined Waste Paper Ash Nanomaterial	WMS: Waste Marble Sludge

Fig. 10 Apparent porosity of the samples according to mixing rates and correlation
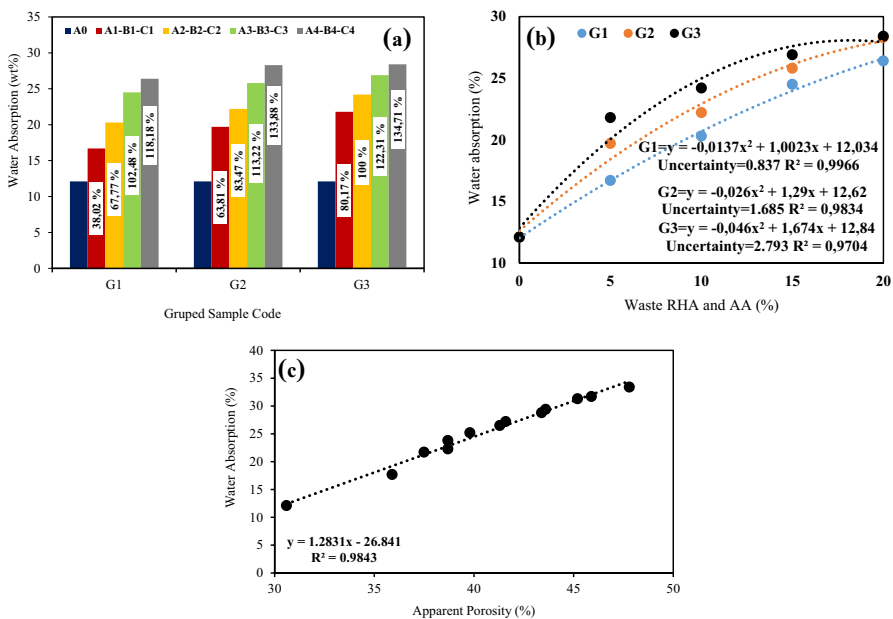

Fig. 11 Water absorption of samples according to mixing rates and correlation

values were calculated using Eq. 6. Wa = Percentage absorption of water by the sample; W_s = soaked weight of the sample after boiling at 100^0C for 2 h; and W_d = dry weight of the sample.

$$W_a = W_s - W_d/W_d \times 100 \qquad (6)$$

The changes in water absorption of the bricks containing waste RHA and KS when compared to the control brick (A0) were submitted as percentages on the bars in the figure. As the values increased, they varied between 12.1 % and 29.4 %. A significant increasing trend was observed in the water absorption capacity of the bricks in the more RHA, KS and alkali activator they contained. A maximum increase of
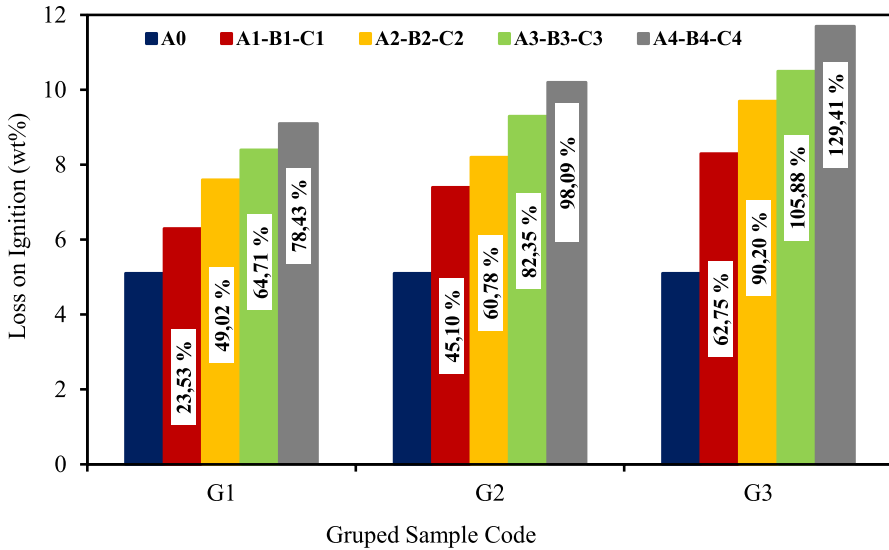
Fig. 12 Loss on ignition of samples

134.71 % was obtained in water absorption capacity of the clay brick at 20 wt% RHA, 30 wt% KS, and 15 wt% AA. A minimum increase of 38.02 % was obtained with addition of 5 wt% RHA, 30 wt% KS, and 5 wt% AA.

Porosity and density influence water absorption capacity significantly. A more porous structure means more water absorption, and ultimately reduces the durability of clay bricks [48]. Referring to Fig. 11 and Table 3, one can see that the addition of RH and AA resulted in a stable increase in porosity. Also, the water absorption range obtained in this study was lower than most of other water absorption ranges cited in the literature (Table 4). If higher rates of RHA, KS, or AA are added during the production of the bricks, then they will become more water absorbent—in turn rendering them useless. The rates used for this study are sufficient to produce this type of brick. In brick standards, the maximum water absorption of first, second, and third class load-bearing wall bricks is 15 %, 19 %, and 23 %, respectively [49, 50]. Brick A1 was within the water absorption limits of the second class group, while bricks A2, B1, B2 and C1 met the water absorption limits of the third class group. These mixtures may be preferred for load bearing applications, while others may be recommended for use in closed environments that are not exposed to water.

3.2.5 Loss on Ignition

The loss on ignition (LOI) values of the fired clay bricks are listed in Table 3 and shown in Fig. 12. They varied between 5.1 wt% and 11.7 wt%. As is shown in Fig. 11, a significant increase was observed in the loss on ignition when the amount of clay reduced and waste RHA and KS were added to the brick structure at different rates. This may be because the waste RHA and KS had a higher LOI (12.4 %) than the raw clay (5.35 %) as shown in Table 1 or because the release of the absorbed water during firing (from the
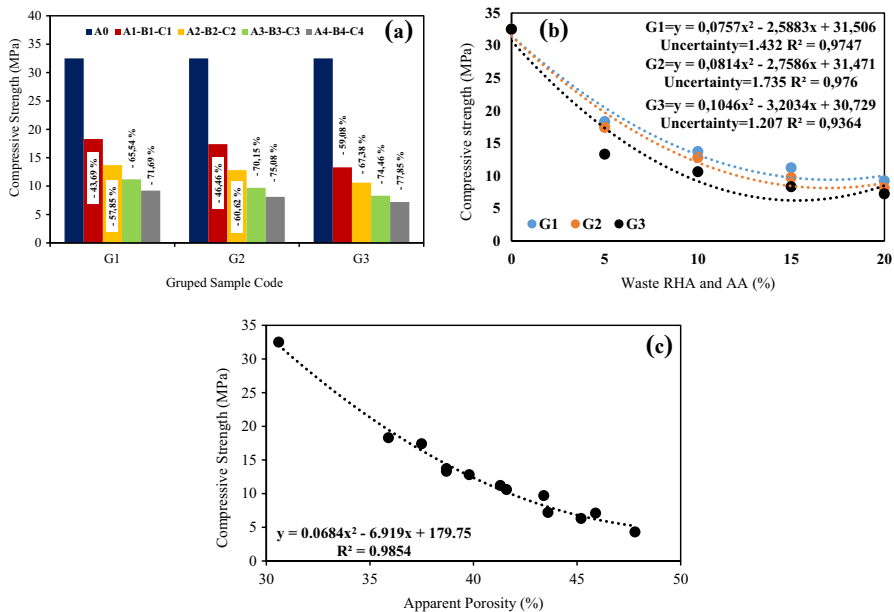
Fig. 13 Compressive strength of samples according to mixing rates and correlation

void) caused by the amount of material that did not react before firing as well as due to dehydroxylation reactions of the minerals, and a combustion reaction of RHA.

3.2.6 Compressive Strength

Compressive strength is a key mechanical property of building bricks and just as a crucial factor for building applications. The compressive strengths of samples are listed in Table 3 and shown in Fig. 13 a. Figure 13 b and c show the correlations between compressive strength, apparent porosity and waste content. As seen in the figure, compressive strength had a negative correlation with apparent porosity and waste content. The changes in the compressive strength of the bricks containing RHA, KS and AA compared to the regular fired clay brick (A0) were given in percentages on the bars in the figure. The values varied between 7.2 MPa and 32.5 MPa. Looking at Fig. 13 a, the compressive strength of the bricks shows a remarkable decrease upon the addition of RH and AA. The sample A1 had the highest compressive strength at about 18.3 MPa with a reduction of 43.69 % compared to the control brick (A0), while the samples B4 and C4 had the lowest compressive strength at 8.1 and 7.2 MPa with decreases of 75.08 % and 77.85 %, respectively. This resulted in a lower degree of geopolymerisation depending on the increase in the SiO_2/Al_2O_3 ratio as the content of RHA increased. This increased the amount of unreacted material which resulted in a looser brick structure, and the resulting microstructure provided a greater porosity and a lower compressive strength. This caused the formation of various weak points within the brick structure as stress concentration centres. The range of compressive strength obtained from this study was higher than most

of the studies in the literature (Table 4). Bricks with low compressive strength are a problem for structural applications, especially in seismic zones; however, they provide an advantage where thermal insulation is required. Pursuant to the brick standards, the compressive strength of first and second class load-bearing wall bricks was min. 15 MPa and 10 Mpa, respectively [51]. Thus, control brick (A0), A1 and B1 bricks met the first-class brick strength limits and the samples A2, A3, B2, C1, and C2 met the second-class brick strength limits. In addition, bricks should have a compressive strength of at least 7 MPa according to European and Turkish standards (TS EN 771–1) [51]. Therefore, even though the compressive strength of all samples decreased, they met the required standards.

3.2.7 Thermal Conductivity

Thermal conductivities of the fired clay bricks are listed in Table 3 and shown in Fig. 14a.

Figures 14 b and c show the correlations between effective thermal conductivity, apparent porosity and waste contents. As seen in the figure, effective thermal conductivity had a negative correlation with apparent porosity and waste content. The changes in effective thermal conductivity of the bricks containing RHA, KS, and AA compared to the control brick (A0) were given in percentages on the bars in the figure. Values varied between 0.263 W·mK^{-1} (C4) and 1.043 W·mK^{-1} (A0).
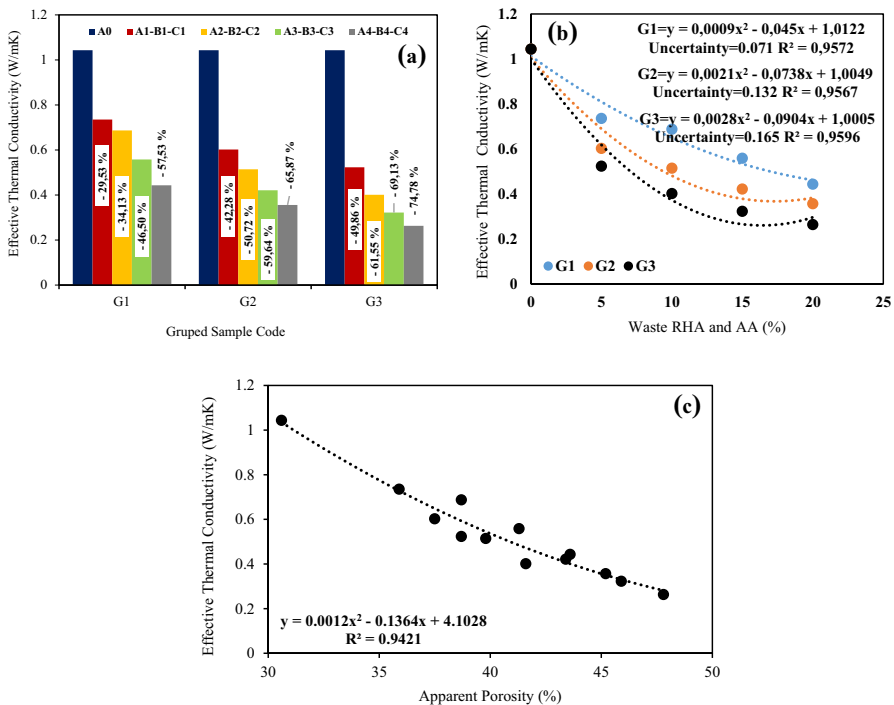

Fig. 14 Effective thermal conductivity of samples according to mixing rates and correlation

The addition of waste RHA to the brick structure at the lowest rate (A1) caused an extreme decrease in the effective thermal conductivity of the fired clay brick (about 29.53 %). When the amounts added reached RHA 20 wt%, KS 30 wt%, and AA 15 wt%, the lowest effective thermal conductivity (0.263 W·mK^{-1}) showed an approximate reduction of 77.78 % compared to the control brick (A0). As the waste RH content increased in the brick, its effective thermal conductivity decreased. The addition of waste RHA into the brick improved its thermal performance. This means that the porous structure of the bricks containing waste RHA traps the air inside and reduces thermal conduction. The effective thermal conductivity results obtained in this study was below average compared to that of other bricks cited in the literature (Table 4). Looking at Fig. 14a, the effective thermal conductivity values of the samples decreased with increasing addition of RHA and AA in all cases. Decreasing effective thermal conductivity values corresponded to increasing porosity as well as decreasing density values in all cases. Likewise, the decrease in the effective thermal conductivity of the samples in this study provided thermal insulation in the buildings and improved the building performance in terms of energy saving. If hollow bricks are made with the compositions in the present study or additional pore-forming agents are added to the brick, thermal conductivities may be more satisfactory. There are no studies performed on the performance of hollow and solid pumice bricks with RHA, KS, and AA. Thus, RHA, KS, and AA-mixed samples were produced and the performance of the bricks was examined in the present study. Reuse of these construction materials used to make clay-based bricks as secondary raw materials affected the technological properties of the bricks (Table 5).

Using waste RHA at different ratios (by weight) and KS powder at a fixed rate as secondary raw material (A1, A2, B1, B2, C1) can be a new method to produce a new material that can be used as a construction material that meets the physical and mechanical properties.

3.3 Microstructure Examination

3.3.1 SEM Analysis of Fractured Brick Materials

Figure 15 shows SEM images of the fractured surfaces of the control bricks and those containing 5 wt% RHA, 30 wt% KS, 5 wt% AA (A1), 10 wt% RHA, 30 wt% KS, 10 wt% AA (B2), 15 wt% RHA, 30 wt% KS, 15 wt% AA (C3), and 20 wt%

Table 5 Summary of the characterization results of the bricks

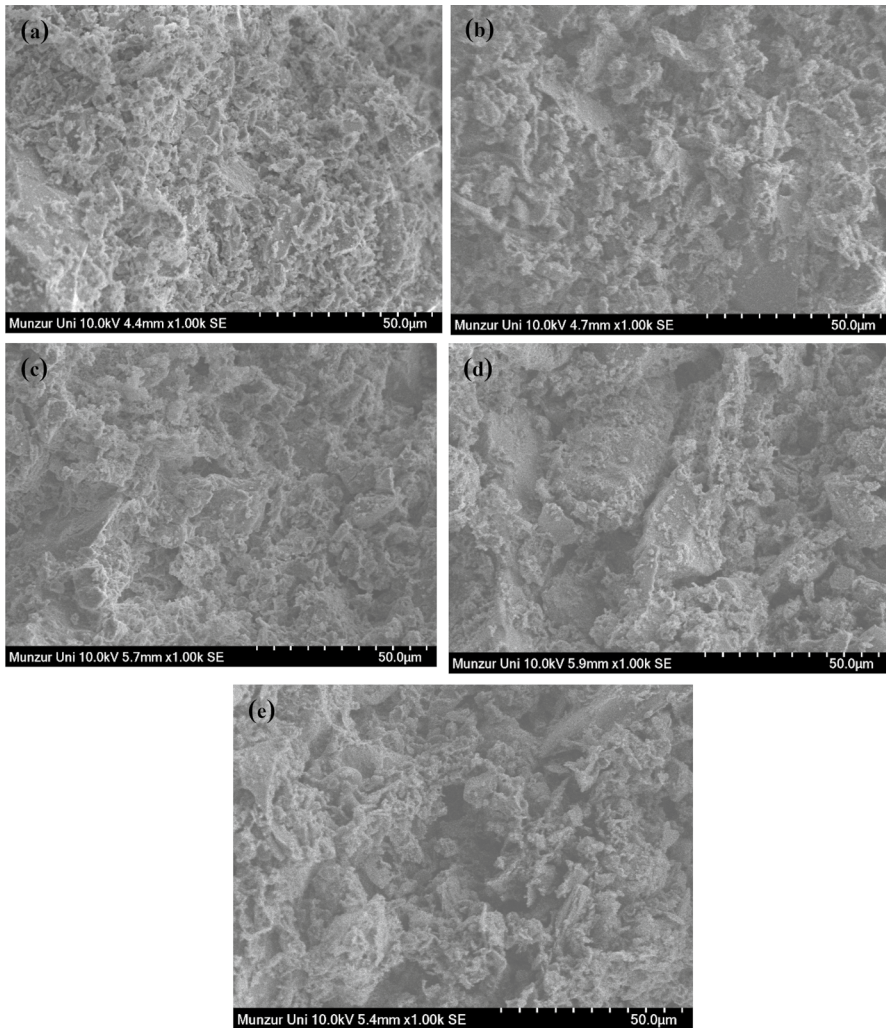| Test	Standard	Requirement	Clay brick (A1, A2, B1, B2, C1)
Shrikange	ASTM	<8 %	3.1–3.5–3.4–3.6–3.7
Apparent porosity	ASTM C373	[20 %–55 %] <40 %	35.9–38.7–37.5–39.8–38.7
Water absorption	ASTM C62	<22 %	16.7–20.3–19.7–22.2–21.8
Bulk density	NF P 94-093	[1.5–1.8] g·cm^{-3}	1.82 to 1.71–1.75–1.62–1.67
Flexural strength	EN 771-1	>7 Mpa	18.3–13.7–17.4–12.8–13.3

Fig. 15 SEM results of fired brick with: a) A0, b) A1, c) B2, d) C3 and e) C4

RHA, 30 wt% KS, and 15 wt% AA (C4). Brick containing 5 wt% RHA, 30 wt% KS, and 5 wt% AA can be selected as the sample with the highest compressive strength. Brick containing 20 wt% RHA, 30 wt% KS, and 15 wt% AA offers the best thermal performance. The SEM images show the porosity remained by the substances that did not react in the brick sample materials because the firing reaction.

   In terms of the fractured surface image, the control brick sample was dense, while the reinforced samples were more porous. The porosity of the samples increased depending on how much additive they contained. Meanwhile, the clay and quartz particles both formed a durable structure due to high temperature during firing, and partially bonded to each other diffusely.

3.3.2 EDS Analysis of Fractured Brick Materials

As is shown in Fig. 16, the brick samples with additives had more and larger porous structure than the control brick. This is attributed to the release of AA from the reaction during firing, the porosity, specific surface size, amorphous structure, and increased amount of unreacted material of RHA. Irregular gaps in the form of micropores were observed in the fired brick structure. The number and size of pores increased with the increasing amount of waste additive. Therefore, bricks containing 20 wt% RHA, 30 wt% KS, and 15 wt% AA had more and larger pores than bricks with 5 wt% RHA, 30 wt% KS, and 5 wt% AA. This was also supported by the results of compressive strength and effective thermal conductivity tests. The results of the superficial EDS analysis of the fractured surfaces of the bricks A1, B2, C3, and C4 are shown in Fig. 16 and listed in Table 6. Si, Al, Fe, Ca, and Mg oxides were observed as main components. EDS analysis showed that the clay had a content compatible with chemical composition of RHA and KS raw materials.

3.3.3 XRD Analysis of Fractured Brick Materials

Figure 17 shows the results of XRD analysis of waste RHA, KS, and AA samples to explain the crystalline phases that formed in the brick samples after firing. The XRD results demonstrate that the samples fired at 950 °C with 5 wt%, 10 wt%, 15 wt%, 20 wt% waste RHA, 30 wt% KS and 5 wt%, 10 wt%, and 15 wt% AA reinforced samples were mainly composed of quartz, albite, hematite, cristobalite, and muscovite crystal phases. The natural mineral components forming the content of the clay became new crystalline phases via high temperature reactions during firing. The quartz phase in the clay content remained undissolved as the main phase in the fired bricks' structure, and created dimensional stability by acting as a filler.

4 Conculusın

This study focused on production of fired bricks that provide thermal insulation by forming pores with varying rates of waste rice husk ash, a fixed rate of Karacadağ scoria, and mixtures supported with chemical reagents. The findings are as follows:

- A significant decrease at a rate of 32.46 % was observed in the bulk density of the clay bricks when the waste RHA content reached 20 wt% and the AA content reached 15 wt%.
- In parallel with the increase in the contents of RHA and AA, the apparent pores of the clay bricks stably increased by 30.6 % to 47.8 %. The porosity increased up to about 56.21 % at the highest RHA and AA content (C4), compared to the control brick (A0).
- The water absorption capacity of the clay bricks also increased by 12.10 wt% to 28.40 wt% (similar to the apparent porosity). A maximum increase of 134.71 % was obtained in the water absorption values of the samples. The samples A1, A2, B1, B2 and C1 met the water absorption limits at the brick standards.
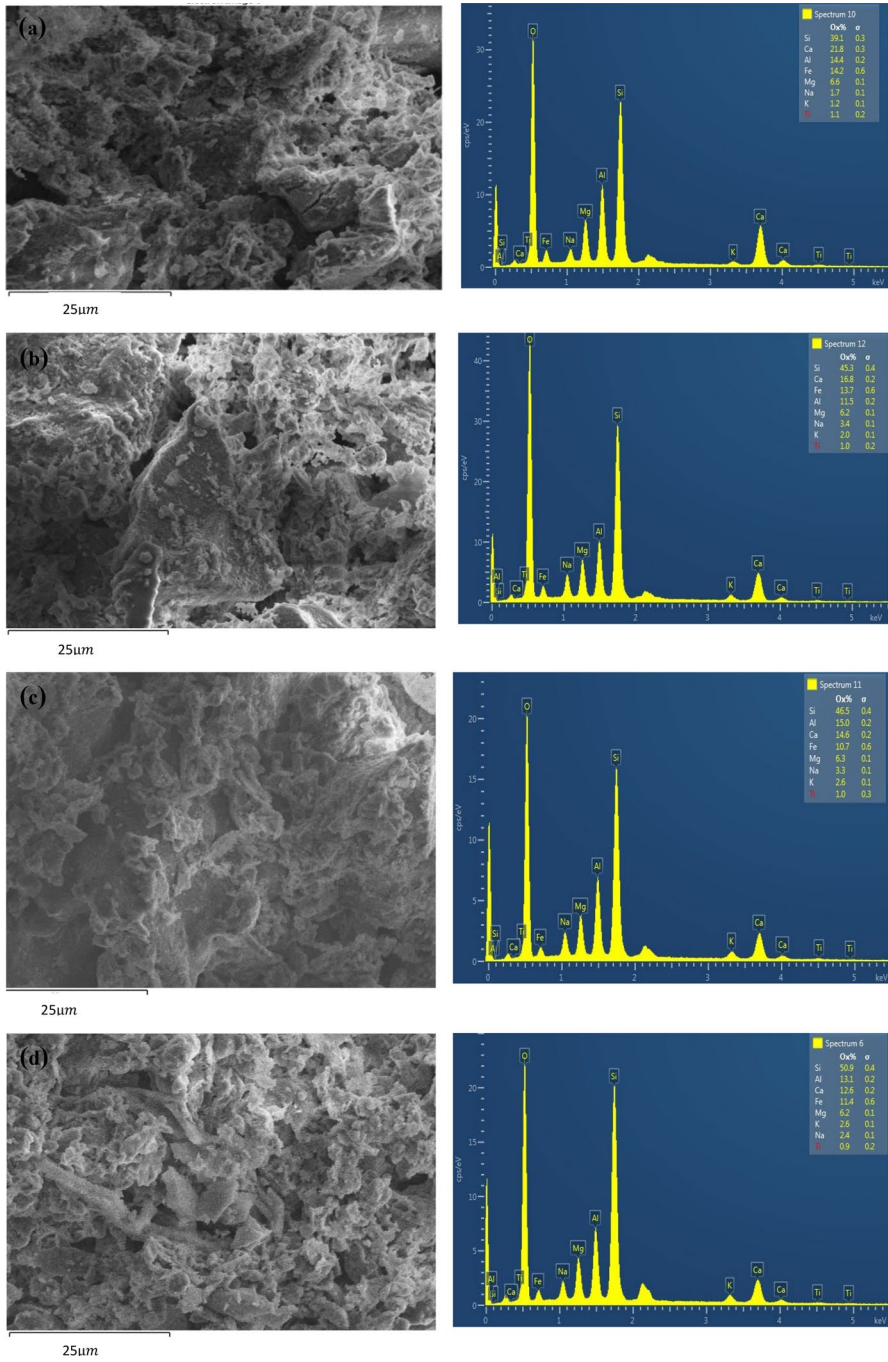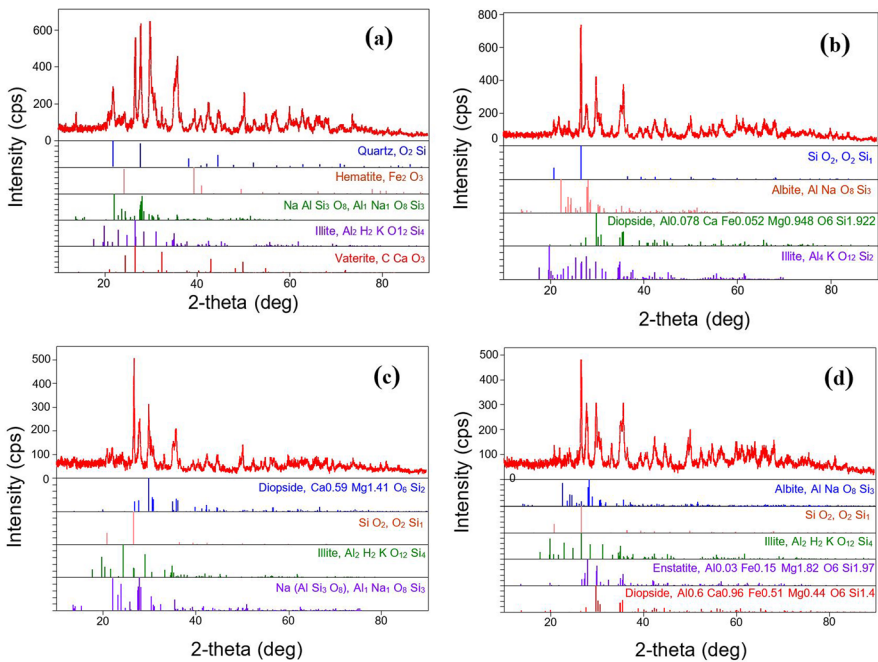
Fig. 16 SEM–EDS results of fired brick with: a) A1, b) B2, c) C3 and c) C4

Table 6 EDS results of the fired clay bricks (wt%)

Element	Sample code			
	A1	B2	C3	C4
Si	39.1	45.3	46.5	50.9
Ca	21.8	16.8	14.6	12.6
Al	14.4	11.5	15.0	13.1
Fe	14.2	13.7	10.7	11.4
Mg	6.6	6.2	6.3	6.2
Na	1.7	3.4	3.3	2.4
K	1.2	2.0	2.6	2.6
Ti	1.1	1.0	1.0	0.9

Fig. 17 XRD result of fired brick with a) A1, b) B2, c) C3 and d) C4

- As the rates of waste RHA, KS, and AA in the brick structure increased, so did the loss on ignition of clay bricks by 5.1 wt% to 11.7 wt%.
- The compressive strength of the clay bricks decreased by 32.5 to 7.2 MPa as the rates of waste RHA and AA in the brick structure increased. All the samples exhibited a compressive strength greater than 7 MPa (as cited in the literature).
- The effective thermal conductivity of the fired clay bricks showed a continuous decreasing trend between 1.043 $W \cdot mK^{-1}$ and 0.263 $W \cdot mK^{-1}$. Even with

the smallest addition of 5 wt% RHA and 5 wt% AA into the clay bricks, their effective thermal conductivity decrease by 29.53 %.

- When the content of waste RHA reached 20 wt% (C4), their effective thermal conductivity dropped sharply by 74.78 %. A significant increase in the thermal performance of the fired clay bricks was observed because of the increase in micropores with the waste RHA rate used.
- C4 exhibited better physical (bulk density, porosity, water absorption and loss on ignition) and thermal performance compared to the other samples, whilst the sample A1 had better mechanical (compressive strength) performance. However, bricks made with other mixture rates also exhibited an acceptable performance. Considering the porosity and effective thermal conductivity results, the use of 20 wt% RHA provided promising results in terms of pore formation.
- The sample A1 in load-bearing structural applications and the sample C4 offer optimum results for structural applications requiring thermal performance.
- Micron-size waste-based pore-forming fired clay bricks featuring RHA, KS and AA appear to offer a great potential to obtain bricks as a wall element in thermal insulation applications. Future studies are recommended to examine approaches through different design of experiments in order to improve the mechanical behaviour of the brick and find a better relationship between mechanical and thermal properties. In addition, the effects of the bricks produced on energy savings, building fuel costs, and CO_2 emission can be analysed.

Declarations

Conflict of interest The author have no conflicts of interest to declare.

References

1. S. Choudhary, M.S. Thakur, N. Dogne, TEQIP-II/Civil/AICMT-2, pp. 5–11 (2014)
2. J. Široký, F. Oldewurtel, J. Cigler, S. Prívara, Appl. Energy **88**(9), 3079–3087 (2011)
3. V. Marinakis, H. Doukas, C. Karakosta, J. Psarras, Appl. Energy **101**, 6–14 (2013)
4. D. Evin, A. Ucar, Appl. Therm. Eng. **154**, 573–584 (2019)
5. M. Sutcu, S. Akkurt, Ceram. Int. **35**, 2625–2631 (2009)
6. S. Ozturk, M. Sutcu, E. Erdogmus, O. Gencel, Constr. Build. Mater. **217**, 592–599 (2019)
7. P. Muñoz, M.P. Morales, M.A. Mendívil, M.C. Juárez, L. Muñoz, Constr. Build. Mater. **71**, 181–187 (2014)
8. C. Arslan, O. Gencel, I. Borazan, M. Sutcu, Erdogmus, E. Constr. Build. Mater. **300**, 124298 (2021)
9. F. Koçyiğit, Int. J. Thermophys. **43**(2), 18 (2022)

10. M. Tapan, Yuzuncu Yıl Univ. J. Sci. Inst. Türkiye, Van **17**, 108–117 (2012)
11. Y. Erdoğan, Master Thesis, Cukurova University Graduated School of Natural and Applied Science, Türkiye, Adana (2007).
12. K.H. Mo, U.J. Alengaram, M.Z. Jumaat, S.P. Yap, S.C. Lee, J. Clean. Prod. **117**, 122–138 (2016)
13. M. Sutcu, J.J. del Coz Díaz, F.P.Á. Rabanal, O. Gencel, S. Akkurt, Energy Build. **75**, 96–108 (2014)
14. G. Görhan, O. Simsek, Build. Mater. **40**, 390–396 (2013)
15. S. Minhaj, S. Kazmi, S. Abbas, M.J. Munir, A. Khitab, J. Build. Eng. **7**, 372–378 (2016)
16. C. Bories, L. Aouba, E. Vedrenne, G. Vilarem, Constr. Build. Mater. **91**, 158–163 (2015)
17. A.M. Heniegal, M.A. Ramadan, A. Naguib, I.S. Agwa, Case Stud. Constr. Mater. **13**, e00397 (2020)
18. F. Anjum, M.Y. Naz, A. Ghaffar, S. Shukrullah, N.M. AbdEl-Salam, K.A. Ibrahim, Physica B **599**, 412479 (2020)
19. N. Benmansour, B. Agoudjil, A. Gherabli, A. Kareche, A. Boudenne, Energy Build. **81**, 98–104 (2014)
20. J. Sutas, A. Mana, L. Pitak, Procedia Eng. **32**, 1061–1067 (2012)
21. D. Eliche-Quesada, M.A. Felipe-Sesé, J.A. López-Pérez, Ceram. Int. **43**(1), 463–475 (2017)
22. S.M.S. Kazmi, S. Abbas, M.L. Nehdi, M.A. Saleem, M.J. Munir, J. Mater. Civ. Eng. **29**(8), 04017056 (2017)
23. J. Balgaranova, A. Petkov, L. Pavlova, E. Alexandrova, Water Air Soil Pollut. **150**, 103–111 (2003)
24. O. Na, Y. Xi, J. Mater. Cycles Waste Manage. **19**(2), 763–773 (2017)
25. O. Gencel, M. Sutcu, E. Erdogmus, V. Koc, V.V. Cay, M.S. Gok, J. Clean. Prod. **59**, 111–119 (2013)
26. I. Quispe, R. Navia, R. Kahhat, Waste Manage. **59**, 200–210 (2017)
27. S. Yıldız, İ Balaydın, Ç. Ulucan, Firat Univ. J. Sci. Eng. Sci. **19**(1), 85–91 (2007)
28. A.N. Givi, S.A. Rashid, F.N.A. Aziz, M.A.M. Salleh, J. Am. Sci. **6**(3), 157–165 (2010)
29. S. Erdoğan, T. Erdoğan, Chem. Add. Structur. Symp., Ankara, Türkiye, pp. 264–329 (2007)
30. B. İşbilir, PhD thesis, Graduate School of Natural and Applied Science, Duzce University (2012)
31. C.L. Hwang, S. Chandra, Noyes Publications, New Jersey (1996)
32. C.L. Hwang, D.S. Wu, *Properties of Cement Paste Containing Rice Husk Ash*, vol. 114 (American Concrete Institute, Farmington, 1989), pp. 733-762 (1989)
33. TS 4790 TSE, Ankara, Turkey (1986)
34. S. Korpayev, M. Bayramov, S. Durdyev, H. Hamrayev, D. Baymyradova, A. Nurmuhammedov, J. Build. Eng. **63**, 105340 (2023)
35. A.M. Heniegal, M.A. Ramadan, A. Naguib, I.S. Agwa, Case Stud. Const. Mater. **13**, e00397 (2020)
36. M.E. Esmeray, M. Atıs, Const. Build. Mater. **194**, 110–121 (2019)
37. N. Phonphuak, M. Teerakun, A. Srisuwan, P. Ruenruangrit, P. Saraphirom, GEOMATE J. **18**(69), 24–29 (2020)
38. F. Anjum, A. Ghaffar, Y. Jamil, M.I. Majeed, J. Mater. Cycl. Waste Manage. **21**, 503–524 (2019)
39. N.L. Bih, A.A. Mahamat, C. Chinweze, O. Ayeni, H.J. Bidossèssi, P.A. Onwualu, E.E. Boakye, Buildings **12**(3), 336 (2022)
40. U.W. Robert, S.E. Etuk, J.B. Emah, O.E. Agbasi, U.A. Iboh, Int. J. Thermophys. **43**(5), 74 (2022)
41. R.D.A. Hafez, B.A. Tayeh, R.O. Abd-Al Ftah, Case Stud. Constr. Mater. **17**, e01391 (2022)
42. M.J. Munir, S.M.S. Kazmi, Y.F. Wu, A. Hanif, M.U.A. Khan, J. Clean. Prod. **174**, 1122–1135 (2018)
43. E. Erdogmus, A. Yaras, M. Sutcu, O. Gencel, Environ. Sci. Pollut. Res. **29**(47), 71936–71947 (2022)
44. G. El Boukili, M. Ouakarrouch, M. Lechheb, F. Kifani-Sahban, A. Khaldoune, Silicon **14**, 4849–4863 (2021)
45. P.M. Velasco, M.P.M. Ortiz, M.A.M. Giró, D.M. Melia, J.H. Rehbein, Appl. Clay Sci. **107**, 156–164 (2015)
46. S. Lawanwadeekul, A. Srisuwan, N. Phonphuak, P. Chindaprasirt, Constr. Build. Mater. **369**, 130547 (2023)
47. Ö. Andiç-Çakır, A.E. Son, S. Sürmelioğlu, E. Tosun, M. Sarıkanat, Case Stud Constr. Mater. **15**, e00560 (2021)
48. F. Koçyiğit, Int. J. Thermophys. **41**(4), 41 (2020)

49. TS EN 771-1, Specification for masonry units—Part 1, Clay Masonry Units (2005)
50. C. Huang, J.R. Pan, K.D. Sun, C.T. Liaw, Water Sci. Technol. **44**(10), 273–277 (2001)
51. Turkish Standard Institution, Specification for masonry units, in *Part 1: Clay Masonry Units*, Ankara, Turkey (2012)

Authors and Affiliations

Şermin Koçyiğit[1]

✉ Şermin Koçyiğit
  serminkocyigit01@gmail.com

[1] Department of Construction Technology, Technical Sciences Vocational School, Dicle University, Diyarbakır, Turkey